Nanoparticles

Deutsche Ausgabe: DOI: 10.1002/ange.201505359
Internationale Ausgabe: DOI: 10.1002/anie.201505359

Mesoscale Characterization of Nanoparticles Distribution Using X-ray Scattering

Cedric J. Gommes, Gonzalo Prieto, Jovana Zecevic, Maja Vanhalle, Bart Goderis, Krijn P. de Jong, and Petra E. de Jongh**

Abstract: *The properties of many functional materials depend critically on the spatial distribution of an active phase within a support. In the case of solid catalysts, controlling the spatial distribution of metal (oxide) nanoparticles at the mesoscopic scale offers new strategies to tune their performance and enhance their lifetimes. However, such advanced control requires suitable characterization methods, which are currently scarce. Here, we show how the background in small-angle X-ray scattering patterns can be analyzed to quantitatively access the mesoscale distribution of nanoparticles within supports displaying hierarchical porosity. This is illustrated for copper catalysts supported on meso- and microporous silica displaying distinctly different metal distributions. Results derived from X-ray scattering are in excellent agreement with electron tomography. Our strategy opens unprecedented prospects for understanding the properties and to guide the synthesis of a wide array of functional nanomaterials.*

Nanoparticles find countless applications in heterogeneous catalysis,[1] in energy storage and conversion devices,[2] in biology and medicine,[3] among others.[4] In many applications the nanoparticles are dispersed on a porous support or embedded in a matrix for the purpose of improving their stability, or to exploit synergistic effects. Understanding the relation between the structure and properties of such complex materials is particularly challenging, first of all from the standpoint of structure characterization at nanometer scale. The properties of nanoparticulate materials depend largely on the characteristics of the particles taken individually. This is the case for their size and shape, which endow the materials with unique thermodynamic,[5] chemical,[6,7] optical,[8] and magnetic[9] properties. In addition, many functionalities are controlled also by collective characteristics of ensembles of nanoparticles. One such characteristic is their spatial distribution at the mesoscopic scale, that is, over distances smaller than about 100 nm, which is attracting an increasing attention in various fields.[10,11] A wide array of phenomena depend critically on distances between particles. This is the case for electromagnetic properties because they generally depend on interference conditions or on the possibility of charge transfer between particles.[12,13] The interparticle distance controls also the stability of nanoparticles towards growth by coalescence or diffusion-limited Ostwald ripening.[11] It was also found that activity and selectivity of a variety of catalysts depend on the spatial distribution of the active nanoparticles at the nanometer scale.[14–17] Understanding all these phenomena, and developing functional nanomaterials that exploit them for specific applications requires the development of efficient and reliable characterization methods.

Experimental methods that can be used to characterize the spatial distribution of nanoparticles at the mesoscopic scale are scarce. The only method that is currently available is electron microscopy. Moreover, because projection effects may significantly bias the apparent interparticle distances, one often relies on electron tomography (3D-TEM).[18–21] Although 3D-TEM provides unique three-dimensional reconstructions of the material with nanometer resolution, it cannot be considered as a final characterization method for several reasons. Many materials cannot withstand the high electron dose required for 3D-TEM without significant structural change. Moreover, electron microscopy is often not suitable for in situ studies, which are indispensible to understand both how a specific nanostructure is formed and how it serves a given function. Finally, another issue of 3D-TEM is the statistical sampling of the technique: the typical mass of material reconstructed by electron tomography is of the order of femtograms. In the case of catalysts, this mass has to be compared with the kilogram or even the ton scale at which the materials are synthesized for industrial applications.[22] This observation calls for the development of bulk characterization techniques to complement and possibly validate 3D-TEM with a macroscopic measurement. In the case of nanoparticle size characterization, it is for that specific purpose that techniques like chemisorption or X-ray diffraction are routinely used.

Herein, we show how small-angle X-ray scattering (SAXS) can be used as a bulk technique to quantitatively characterize the mesoscale spatial distribution of supported nanoparticles. We illustrate this point for supported copper catalysts, which are relevant for many chemical processes such as methanol synthesis,[11] biomass processing[23] and solar fuels production.[24] Two Cu/SiO_2 catalysts were synthesized by impregnation of SBA-15 ordered porous silica[25] with an

[*] C. J. Gommes
Department of Chemical Engineering, University of Liège
Allée du 6 août 3, 4000 Liège (Belgium)
E-mail: cedric.gommes@ulg.ac.be
G. Prieto, J. Zecevic, K. P. de Jong, P. E. de Jongh
Debye Institute for Nanomaterials Science
Utrecht University
Universiteitsweg 99, 3584 CG Utrecht (The Netherlands)
E-mail: P.E.deJongh@uu.nl
M. Vanhalle, B. Goderis
Polymer Chemistry and Materials
Catholic University of Leuven
Celestijnenlaan 200F, 3001 Heverlee (Belgium)

Supporting information for this article is available on the WWW under http://dx.doi.org/10.1002/anie.201505359.

aqueous solution of copper nitrate, followed by drying and two different heat treatments (see the Supporting Information). For the first catalyst (Cu/SBA-15/N2) the heat treatment was done in nitrogen flow, favoring the homogeneous distribution of nanoparticles. The second catalyst (Cu/SBA-15/NO) was obtained in a flow of nitrogen and nitric oxide, resulting in the formation of high-density domains of nanoparticles.[26] The two catalysts were first characterized by electron tomography. The results are summarized in Figure 1,

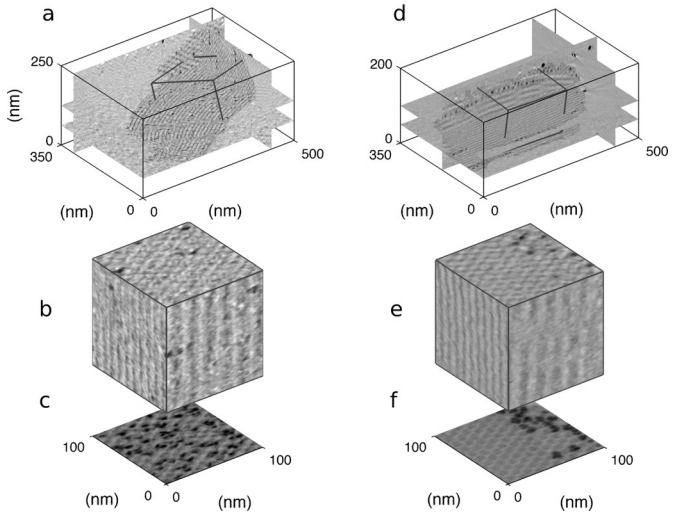

Figure 1. Electron tomography reconstructions of catalysts Cu/SBA-15/N2 (left, a to c) and Cu/SBA-15/NO (right, d to f) showing different spatial distributions of the copper nanoparticles: a,d) complete grain, b,e) selected cube oriented along the mesopores, c,f) projection of the cube in which copper-containing mesopores are darker.

while full tomograms are given as movies S1 and S2 in the Supporting Information. Despite the overall copper loading being $0.18\,g_{Cu}/g_{SiO_2}$ in both materials, the different spatial distributions of the Cu nanoparticles are clear from the tomographic reconstructions. This is highlighted in Figure 1 by extracting $(100\,nm)^3$ cubes from the tomograms and projecting them along the direction of the mesopores, which reveals the nanoparticles present in any individual mesopore. In Cu/SBA-15/N2 copper nanoparticles are present in almost all mesopores (Figure 1 c). In the case of Cu/SBA-15/NO the nanoparticles gather into only a small fraction of the mesopores, while most of them are left empty (Figure 1 f).

In addition to testifying to the power of electron tomography, Figure 1 illustrates also the poor statistical sampling. Assuming a density of $1\,g\,cm^{-3}$, typical of porous silica, the $(100\,nm)^3$ volume corresponds to a mass of 10^{-15} g, hence our referring to 3D-TEM as a femtogram technique. Relying exclusively on 3D-TEM to understand structure–property relationships of nanostructured materials would be a leap of faith. Bulk characterization methods are therefore necessary to test the homogeneity of the nanostructure on a macroscopic scale. In that spirit, the small-angle X-ray scattering (SAXS) patterns of the materials of Figure 1 were also measured. They are plotted in Figure 2 against the scattering vector q. As a rule of thumb, the scattering vector q

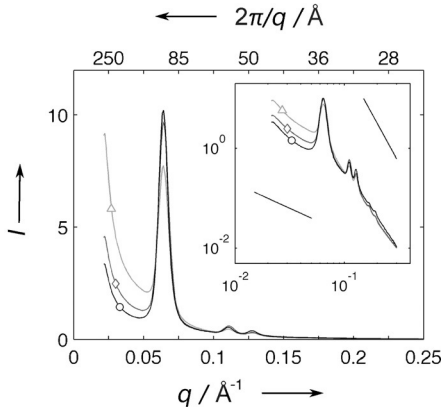

Figure 2. Small-angle X-ray scattering (SAXS) patterns of empty SBA-15 support (○) as well as of catalysts Cu/SBA-15/N2 (◇), and Cu/SBA-15/NO (△). The same data is plotted in the inset on double logarithmic scales: the two lines are power laws of the type $I \approx q^{-4}$ and $I \approx q^{-1}$.

converts to a characteristic length l of the structure by the inverse relation $l = 2\pi/q$ (see the Supporting Information).[27] Therefore, the scattering in the q-range from 0.02 to 0.2 $Å^{-1}$ corresponds to structures with sizes ranging from approximately 3 to 30 nm, which roughly matches those of the 3D-TEM reconstructions. A striking difference between the two techniques, however, is the milligram of material characterized by SAXS. This corresponds to a twelve-decade enhancement compared to electron tomography. For comparison the SAXS pattern of the empty SBA-15 support, that is, before impregnation with copper nitrate, is also shown in Figure 2.

The SAXS patterns of the two catalysts and of the empty support exhibit the characteristic Bragg peaks of SBA-15-ordered mesoporous silica, corresponding to the hexagonal P_{6mm} symmetry of the mesopore lattice.[28] The position and width of the peaks are the same for all materials, suggesting that the porous support was not damaged by the impregnation and subsequent heat treatments. They convert to a 10 nm spacing between neighboring mesopores, and to a grain size of 100 nm according to the Scherrer equation.[27] The former value compares reasonably with the tomographic reconstructions in Figure 1. The latter underestimates the actual size of the grains, which is close to 300 nm according to electron microscopy, thereby hinting at a significant strain broadening of the peaks.[27,29] Interestingly, the main difference between the SAXS of the various samples is the intensity of the background scattering, which is mostly apparent below $q \approx 0.05$ $Å^{-1}$. The background of Cu/SBA-15/NO is about two times more intense than Cu/SBA-15/N2, and three times more intense than the empty SBA-15 support.

In order to analyze the intensity of the background scattering in terms of the material nanostructure, consider first the case of the empty SBA-15 support. If the material consisted of a perfectly periodic and infinite array of identical mesopores carved in an otherwise homogeneous solid, complete destructive interference would occur for any value of q not satisfying Bragg's condition. There would therefore be no background in the scattering pattern. It is the deviation of the actual nanostructure from perfect periodicity that is

responsible for the background.[27,29] In the case of SBA-15 there are three contributions. First, the material between the mesopores is not a homogeneous solid because it contains micropores with a disordered structure.[30] Second, the mesopores all have slightly different sizes, and their positions deviate randomly from the nodes of the perfect hexagonal lattice.[28,31] Third, the hexagonal lattice does not extend infinitely because the material comes in grains a few hundred nanometers across (see Figure 1). In addition to that, in the case of the copper-loaded catalysts, any non-uniformity in the metal loading among the mesopores would make the overall structure less periodic and would accordingly contribute to the background. With this qualitative interpretation in mind, the SAXS data in Figure 2 suggest that the copper distribution is well-nigh homogeneous in Cu/SBA-15/N2 because the background is barely larger than in the empty SBA-15 support. By contrast, the high background intensity in Cu/SBA-15/NO hints at a heterogeneous copper distribution within that catalyst. These observations agree qualitatively with the 3D-TEM reconstructions in Figure 1.

In order to make the scattering data analysis quantitative, all the mentioned structural deviations from periodicity have to be accounted for. Our modelling approach is sketched in Figure 3: each of the three structural levels of the SBA-15

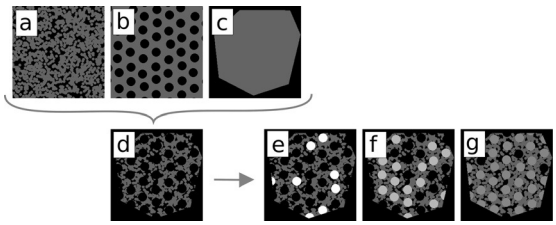

Figure 3. Modelling methodology used to analyze X-ray scattering from copper catalysts supported on SBA-15 silica: a) the microporous, b) mesoporous, and c) grain structures are combined into a comprehensive model of the support (d). The spatial distribution of the metal is then modelled by randomly allowing a prescribed fraction Λ of the mesopores to hold metal: e) 20, f) 50 or g) 80%. The gray tone symbolizes the average density of the pore-filling material, which is adjusted to ensure a constant overall metal loading.

support—the micropores (a), the mesopores (b) and the grain itself (c)—is modelled independently and subsequently combined into a single and comprehensive structural model of the support (d). The heterogeneity of the nanoparticles distribution is then modelled by allowing each mesopore to be loaded with copper with a prescribed loading probability Λ. For, say $\Lambda = 0.2$, all the metal nanoparticles are statistically gathered into only 20% of the mesopores, chosen randomly, resulting in a very heterogeneous spatial distribution (Figure 3e). By contrast, the value $\Lambda = 1$ represents a homogeneous distribution of the nanoparticles over all the mesopores.

We show in the Supporting Information that the small-scale structure of the copper, namely that it comes in the form of nanoparticles, has a minor impact on the background intensity for values of q below $q \approx 0.05$ Å^{-1}. For convenience, the metal loading is therefore modelled as a homogeneous phase filling entirely the loaded mesopores, and the density of which is adjusted to comply with the known overall metal loading of the catalysts. The relevant density for X-ray scattering is the number of electrons per unit volume. In Figure 3e to g, different gray tones are used to symbolize the adjustment of the mesopore-filling material density for different values of Λ. The mathematical expression for the SAXS intensity of the model sketched in Figure 3, with or without metal, is rigorously derived in the Supporting Information starting from the first principles of X-ray scattering theory.[27]

The aim of our scattering data analysis is to determine the values of the loading probability Λ relevant to catalysts Cu/SBA-15/N2 and Cu/SBA-15/NO. This is equivalent to quantifying the mesoscale heterogeneity of the metal distribution. For that purpose it is necessary to analyze first the scattering of the empty SBA-15 support. The structural model sketched in Figure 3d is described in detail in the Supporting Information. It comprises six structural parameters, namely the diameter of the grains considered as elongated cylinders, the spacing between mesopores, their average diameter as well as the breadth of their size distribution, the average micropore size and their volume fraction, corresponding to the porosity of the wall between the mesopores. For the SAXS analysis, the diameter of the grains was fixed to 300 nm in agreement with microscopy (see Figure 1) and the porosity of the wall was fixed to 35%, which is derived from nitrogen physisorption studies[31] and is confirmed by the mechanical properties of SBA-15.[33] The remaining structural parameters were obtained by the least-square fit of the scattering data. The best fit is shown in Figure 4a together with a realization of the model based on the fitted parameters. The three contributions to the background scattering—micropores, mesopore polydispersity, and finite grain size—are also shown in Figure 4a. These contributions are of comparable intensity, which means that the latter three structural levels in SBA-15 are of equal importance for the SAXS data analysis. The visual similarity between the realization of the model and tomographic reconstructions of SBA-15 is striking.[29] Moreover the mesoporous volume determined from the SAXS analysis of the empty SiO_2 support ($V_p = 0.7\ cm^3\,g^{-1}$ see Supporting Information) is identical to the value obtained independently by nitrogen adsorption at the same material, which shows that the model realistically captures the main features of the support.

As the nanostructure of the SBA-15 support itself is not modified by the impregnation by copper nitrate and further heat treatments, the SAXS of the copper-loaded catalysts were fitted with the loading probability Λ as a single adjustable parameter. The best fits of the scattering patterns of Cu/SBA-15/N2 and Cu/SBA-15/NO are shown in Figure 4b and c, together with realizations of the model. In the case of the catalyst calcined in nitrogen, the fitting of the SAXS shows that the copper is homogeneously distributed over 74% of the mesopores ($\Lambda = 0.74$). Based on the overall copper loading, this value means that in each copper-containing mesopore the metal nanoparticles themselves occupy about 4% of the pore volume. By contrast, in the catalyst calcined in the presence of NO the copper loading is heterogeneous and the copper concentrates in only about 11% of all mesopores ($\Lambda = 0.11$).

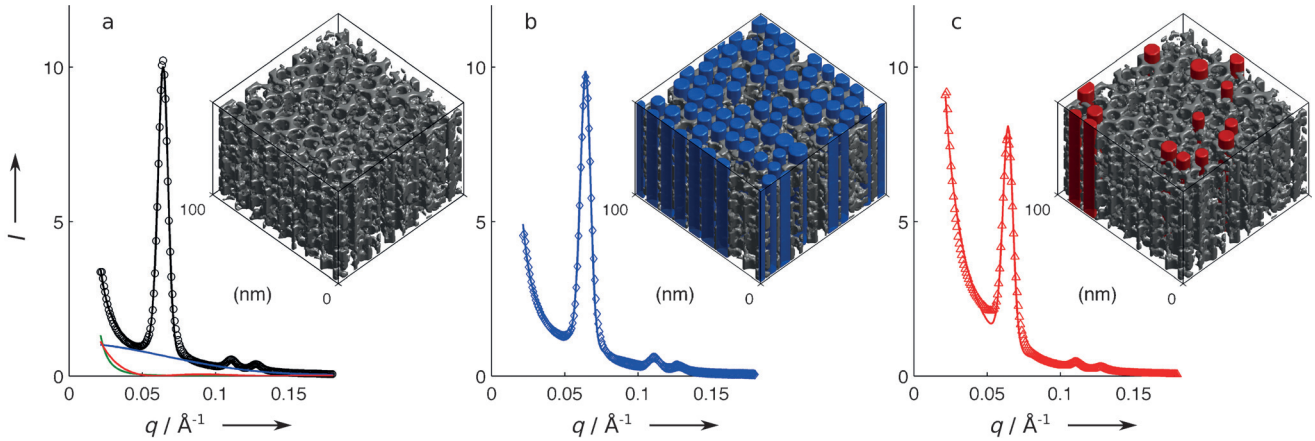

Figure 4. Small-angle X-ray scattering patterns of a) the empty SBA-15 support and of b) copper-loaded samples Cu/SBA-15/N2 and c) Cu/SBA-15/NO: the symbols are the experimental data and the solid lines are the fits. The insets are realizations of the structural model with parameters derived from the SAXS, with the copper-containing mesopores highlighted as colored cylinders. The color lines in panel (a) are the three contributions to the background scattering of the empty SBA-15 support, namely the micropores (blue), the mesopore polydispersity (red), and the finite grain size (green).

In each of these mesopores, the copper particles occupy about 26% of the available volume.

It is truly remarkable that the intensity of the background scattering can provide such detailed information about the spatial distribution of the nanoparticles in the SBA-15 support. The visual similarity between Figures 1 and 4 is striking despite a difference in twelve orders of magnitude in the sampling between the two techniques: a femtogram of material for 3D-TEM and a milligram for X-ray scattering. The improvement in sampling is made possible through a conceptual change, that is, by using a probabilistic approach for microstructure characterization. In that respect, the insets of Figure 4 do not correspond to actual structures present in the materials. They represent particular realizations of a more general probabilistic model, which captures both the complexity and the variability of the nanostructure over the entire aliquot of material sampled by the X-ray scattering technique.

The present work has numerous ramifications in the field of nanostructured materials in general, with potential applications to the structural analysis of, for example, catalysts, energy conversion and storage devices, and photonic materials. Many phenomena relevant to these applications depend critically on the spatial distribution of nanoparticles at the mesoscopic scale. In addition to improving the statistical sampling by twelve decades compared to existing electron tomography methods our work also paves the way to a wealth of in situ scattering studies, which are often indispensable to understand both how a given nanostructure forms and how it serves a specific function.

Acknowledgements

C.J.G. is a research associate at the Funds for Scientific Research (F.R.S.-FNRS Belgium).

Keywords: catalysts · electron tomography · nanoparticles · small-angle X-ray scattering · spatial distribution

How to cite: *Angew. Chem. Int. Ed.* **2015**, *54*, 11804–11808
Angew. Chem. **2015**, *127*, 11970–11974

[1] A. T. Bell, *Science* **2003**, *299*, 1688–1691.
[2] C. Liu, F. Li, M. Lai-Peng, H.-M. Cheng, *Adv. Mater.* **2010**, *22*, E28–E62.
[3] M. De, P. S. Ghosh, V. M. Rotello, *Adv. Mater.* **2008**, *20*, 4225–4241.
[4] H. Goesmann, C. Feldmann, *Angew. Chem. Int. Ed.* **2010**, *49*, 1362–1395; *Angew. Chem.* **2010**, *122*, 1402–1437.
[5] M. Paskevicius, D. A. Sheppard, C. E. Buckley, *J. Am. Chem. Soc.* **2010**, *132*, 5077–5083.
[6] J. P. den Breejen, P. B. Radstake, G. L. Bezemer, J. H. Bitter, V. Frøseth, A. Holmen, K. P. de Jong, *J. Am. Chem. Soc.* **2009**, *131*, 7197–7203.
[7] S. E. F. Kleijn, S. C. S. Lai, M. T. M. Koper, P. R. Unwin, *Angew. Chem. Int. Ed.* **2014**, *53*, 3558–3586; *Angew. Chem.* **2014**, *126*, 3630–3660.
[8] K. L. Kelly, E. Coronado, L. L. Zhao, G. C. Schatz, *J. Phys. Chem. B* **2003**, *107*, 668–677.
[9] A.-H. Lu, E. L. Salabas, F. Schüth, *Angew. Chem. Int. Ed.* **2007**, *46*, 1222–1244; *Angew. Chem.* **2007**, *119*, 1242–1266.
[10] Y. Zhao, K. Thorkelsson, A. J. Mastroianni, T. Schilling, J. M. Luther, B. J. Rancatore, K. Matsunaga, H. Jinnai, Y. Wu, D. Poulsen, J. M. J. Fréchet, A. P. Alivisatos, T. Xu, *Nat. Mater.* **2009**, *8*, 979–985.
[11] G. Prieto, J. Zečević, H. Friedrich, K. P. de Jong, P. E. de Jongh, *Nat. Mater.* **2013**, *12*, 34–39.
[12] C. Petit, Z. L. Wang, M. P. Pileni, *J. Magn. Magn. Mater.* **2007**, *312*, 390–399.
[13] S. K. Ghosh, T. Pal, *Chem. Rev.* **2007**, *107*, 4797–4862.
[14] A.-H. Lu, J.-J. Nitz, M. Comotti, C. Weidenthaler, K. Schlichte, C. W. Lehmann, O. Terasaki, F. Schüth, *J. Am. Chem. Soc.* **2010**, *132*, 14152–14162.
[15] B. Wickman, Y. E. Seidel, Z. Jusys, B. Kasemo, R. J. Behm, *ACS Nano* **2011**, *5*, 2547–2558.
[16] P. Munnik, P. E. de Jongh, K. P. de Jong, *J. Am. Chem. Soc.* **2014**, *136*, 7333–7340.
[17] S.-I. Naya, T. Niwa, T. Kume, H. Tada, *Angew. Chem. Int. Ed.* **2014**, *53*, 7305–7309; *Angew. Chem.* **2014**, *126*, 7433–7437.
[18] C. J. Gommes, K. de Jong, J.-P. Pirard, S. Blacher, *Langmuir* **2005**, *21*, 12378–12385.

[19] H. Friedrich, J. R. Sietsma, P. E. de Jongh, A. Verkleij, K. P. de Jong, *J. Am. Chem. Soc.* **2007**, *129*, 10249 – 10254.
[20] E. P. W. Ward, T. J. V. Yates, J. J. Fernández, D. E. W. Vaughan, P. A. Midgley, *J. Phys. Chem. C* **2007**, *111*, 11501 – 11505.
[21] J. Zečević, K. P. de Jong, P. E. de Jongh, *Curr. Opin. Solid State Mater. Sci.* **2013**, *17*, 115 – 125.
[22] S. Mitchell, N.-L. Michels, J. Pérez-Ramírez, *Chem. Soc. Rev.* **2013**, *42*, 6094 – 6112.
[23] B. J. O'Neill et al., *Angew. Chem. Int. Ed.* **2013**, *52*, 13808 – 13812; *Angew. Chem.* **2013**, *125*, 14053 – 14057.
[24] K. P. Kuhl, E. R. Cave, D. N. Abram, T. F. Jaramillo, *Energy Environ. Sci.* **2012**, *5*, 7050 – 7059.
[25] C. T. Kresge, M. E. Leonowicz, W. J. Roth, J. C. Vartuli, J. S. Beck, *Nature* **1992**, *359*, 710 – 712.
[26] P. Munnik, M. Wolters, A. Gabrielsson, S. D. Pollington, G. Headdock, J. H. Bitter, P. E. de Jongh, K. P. de Jong, *J. Phys Chem. C* **2011**, *115*, 14698 – 14706.
[27] D. S. Sivia, *Elementary Scattering Theory: For X-ray and Neutron Users*, Oxford University Press, New York, **2011**.
[28] M. Impéror-Clerc, P. Davidson, A. Davidson, *J. Am. Chem. Soc.* **2000**, *122*, 11925 – 11933.
[29] S. Förster, A. Timmann, M. Konrad, C. Schellbach, A. Meyer, S. S. Funari, P. Mulvaney, R. Knott, *J. Phys. Chem. B* **2005**, *109*, 1347 – 1360.
[30] M. Kruk, M. Jaroniec, C. H. Ko, R. Ryoo, *Chem. Mater.* **2000**, *12*, 1961 – 1968.
[31] C. J. Gommes, H. Friedrich, M. Wolters, P. E. de Jongh, K. P. de Jong, *Chem. Mater.* **2009**, *21*, 1311 – 1317.
[32] H. Brumberger, J. Goodisman, R. Ramaya, S. Ciccariello, *J. Appl. Crystallogr.* **1996**, *29*, 526 – 530.
[33] J. Prass, D. Müter, P. Fratzl, O. Paris, *Appl. Phys. Lett.* **2009**, *95*, 083121.

Received: June 11, 2015
Published online: August 10, 2015

